# Adaptive Sampling Limit Surface Search Application to Identify Cliff-Edge Effects in Severe Accident Uncertainty Analysis

Pietro Maccari,[a]* Andrea Bersano,[b] Fabrizio Gabrielli,[c] and Fulvio Mascari[b]

[a]*ENEA, Nuclear Department (NUC), NUC-ING, C.R. Brasimone, Italy*
[b]*ENEA, Nuclear Department (NUC), NUC-SICNUC, Bologna, Italy*
[c]*KIT, Reactor Physics and Dynamic (RPD) Group, Hermann-von-Helmholtz-Platz, 1, Karlsruhe, Germany*

**Abstract** — *Severe accident (SA) codes and their core degradation models have to deal with strongly nonlinear and discontinuous phenomena. In the application of uncertainty quantification to SA simulations, the combination of such phenomena may lead to a strong increase in the uncertainty propagated through the simulation, as well as to the chaotic behavior of the output variables. In this framework, the application of the limit surface search method of the RAVEN tool is proposed for a case where cliff-edge effects of SA phenomena determine a bifurcation of an output figure of merit. The algorithm is based on a predictive method making use of a support vector machine model, and it is applied with the aim of separating those input values that lead to different phenomenologies among the uncertainty calculations. The case study is in regard to the uncertainty analysis of the ASTEC code simulation of the QUENCH6 experimental test conducted in the framework of the International Atomic Energy Agency Coordinated Research Project I31033.*

**Keywords** — *Machine learning, adaptative sampling, severe accident, uncertainty quantification, ASTEC.*

## I. INTRODUCTION

### I.A. Generalities

Nowadays, the nuclear safety community extensively relies on numerical simulation codes to analyze postulated accidents in nuclear power plants (NPPs). Such tools are employed as key elements in assessing compliance with safety requirements. Among these, severe accident (SA) codes have been developed with the capability to integrate reactor thermal-hydraulic simulations with core degradation, fission product transport, and other relevant SA phenomena. SA codes are being used for the assessment of accident management measures aimed at preventing and mitigating the consequences of a SA. In addition, extensive applications in industrial, regulatory, and research areas can be found.[1] Among the most used and mentioned SA codes are Accident Source Term Evaluation Code (ASTEC),[2] MAAP,[3] and MELCOR.[4]

Because of the growing maturity and interest in such codes, the nuclear research community has recently started to investigate the uncertainty embedded in them by taking advantage of strategies and tools already consolidated for thermal-hydraulic analysis. Therefore, the best-estimate plus uncertainty approach[5,6] has started to be used in SA code analyses.

Among the international research projects applying the state-of-the-art of uncertainty quantification (UQ) to SA simulations are the MUSA (Management and Uncertainties of Severe Accidents) project,[7] and in parallel, the

*E-mail: pietro.maccari@enea.it

International Atomic Energy Agency Coordinated Research Project (CRP) I31033, "Advancing the State-of-Practice in Uncertainty and Sensitivity Methodologies for SA Analysis in Water Cooled Reactors."[8,9] In this framework, the application of the probabilistic propagation of input uncertainties method has been the most commonly used for numerical simulations.[5,10] In this case, some peculiarities of the SA codes have been highlighted within many UQ applications, and often, critical issues have arisen.

### I.B. Output Bifurcations and Cliff-Edge Effects in SA Simulations

Because of the intrinsic nature of the involved phenomena, SA codes and their models have to deal with strongly nonlinear and discontinuous phenomena: with the exponential acceleration of Zircaloy oxidation, the noncontinuous degradation, failure, and relocation of core components, and the explosive pressure increase consequent to a corium-water interaction just a few examples of the nonlinear and discontinuous phenomena that SA codes have to deal with.

The combination of such phenomena in a sequence may lead to a quick increase in the uncertainty propagated through the simulation. For this reason, in the application of the probabilistic propagation of input uncertainties method, a general spread of uncertainty among the several calculations is often observed. And in addition, a chaotic and discontinuous behavior of the output figures of merit (FOMs) may take place.

As an example, in the UQ study carried out in Ref. [11], a discontinuous behavior of the output was observed with respect to the variation of an uncertain input parameter. In Refs. [12–14], bifurcations of the output FOMs and a general uncertainty spread in the results were observed. In particular, in the UQ application carried out in Ref. [15], a cliff-edge effects deriving from the bifurcation of a specific core degradation phenomenon was assessed.

### I.C. Motivation of Limit Surface Search Application

The probabilistic propagation of input uncertainties method is based on the so called Wilks confidence interval formula,[16,17] which is a statistical criteria used to choose the minimum number of code calculations required to have enough confidence in the results.[5,10] A key point for the present work was that, as well assessed in Ref. [18], to guarantee the statistics of the Wilks formula, the assumption should be made that the code model does not show chaotic behavior, which can be easily attributed to those systems in which a bifurcation of the output domain is observed.

In the case of the occurrence of bifurcations in UQ applications to a SA sequence, the present paper proposes the use of the limit surface (LS) research method as a supporting approach to address such a case. In this context, this method can be employed to identify the input parameter values that lead to different simulated phenomena. Consequently, it may be possible to consider the Wilks formula as applicable to more restricted input domains, i.e., those identified by the determined LS.

## II. METHODOLOGY

### II.A. Uncertainty and Sensitivity Analysis

#### *II.A.1. Theoretical Basis: Black Box Model and Chaotic Behavior*

A code model of a NPP is a complex system characterized by input data (e.g., material and geometric data, boundary conditions) that is able to calculate an output response in terms of output physical parameters. Due to its complexity, the code simulation can be seen as a black box represented by a nonlinear deterministic operator $L(t)$ mapping the input random vector $\vec{x}$ into an output vector $\vec{y}(t)$,

$$\vec{y}(t) = L(t)\vec{x} \quad . \tag{1}$$

Considering the input vector $\vec{x}$ as a stochastic variable varying according to a probability distribution function (PDF), $\vec{y}$ is also a random variable with an associated PDF.[18] In this sense, we call $X$ the set of all possible values of $\vec{x}$, and $Y$ will be its image in the output space given by the mapping through $L(t)$.

According to Refs. [18,19], we can speak of the chaotic behavior of the system when its output space ends up being the union of disjoint sets. Or in other words, if in some points of the input set $X$ (bifurcation points $\overrightarrow{x_{bi}} \in X$), the gradient assumes different values depending on the direction of approach to the point, i.e.,

$$\frac{\vec{y}\left(\overrightarrow{x_{bi}} + \delta\overrightarrow{x_1}\right) - \vec{y}\left(\overrightarrow{x_{bi}}\right)}{\left|\delta\overrightarrow{x_1}\right|} \neq \frac{\vec{y}\left(\overrightarrow{x_{bi}} + \delta\overrightarrow{x_2}\right) - \vec{y}\left(\overrightarrow{x_{bi}}\right)}{\left|\delta\overrightarrow{x_2}\right|} \quad . \tag{2}$$

Therefore, when chaos is present, the input set can be divided into subsets as well ($X = \cup_{i=1}^{n} X_i$) such that the mapping operator $L(t)$ will be the same and smooth in each subset $X_i$, but it will vary when passing from one subset to

another. A schematic representation of nonchaotic and chaotic system behaviors is reported in Fig. 1.

This can also give hints on the detection of chaotic behavior in the framework of the code simulations, which, according to Ref. [18], takes place when the following three conditions are simultaneously satisfied:

1. The output average value considerably changes.
2. The output variance suddenly increases.
3. The output variables tend to separate into disjoint groups.

### II.A.2. Theoretical Basis: Wilks Confidence Interval Formula

Considering the previous definitions, the scope of the Wilks confidence interval formula is to provide a statistical criterion to have enough information on the output set $Y$ with a random sampling of a limited number of calculations. A key point for the present work is that, according to Ref. [18], an assumption on which the formula is based is that the mapping $L(t)$, representing the code, does not show chaotic behavior.

Within this assumption, the simplest case of scalar output variable $y$, with its PDF being $g(y)$ can be considered. Carrying out $N$ code runs with $N$ random inputs $\{\overrightarrow{x_1}, \overrightarrow{x_2}, \ldots, \overrightarrow{x_N}\} \in X$, a sample of the output variable $\{y_1, y_2, \ldots, y_N\}$ is obtained. Let us now consider the two random functions $L(y_1, y_2, \ldots, y_N)$ and $U(y_1, y_2, \ldots, y_N)$, called, respectively, the lower and upper tolerance limits. Hence, attributing to $P$ the meaning of probability, we can write

$$P\left\{\int_L^U g(y)dy > \gamma\right\} = \beta \quad . \tag{3}$$

This relation defines the probability β, which we call the confidence level, such that the portion of the output distribution $g(y)$ included in the tolerance limits $L$ and $U$ is greater than the number γ, called the probability content. Therefore, having fixed the values of γ and β (in the $[0, 1]$ interval), the Wilks formula can be used to determine the number of runs $N$, from which we can determine an appropriate tolerance interval $[L, U]$. Indeed, in its work,[16,17] Wilks proved that the probability that $\int_L^U g(y)dy > \gamma$ holds is equal to

$$\beta = \sum_{j=0}^{s-r-1} \frac{N!}{(N-j)!j!}\gamma^j(1-\gamma)^{N-j} \quad , \tag{4}$$

defining $r$ and $s$ such that $0 \le r \le s \le N$, $L = y(r)$, and $U = y(s)$.

From this, the two-sided tolerance interval formula can be derived by selecting the tolerance limits $L = y(r = 1)$ and $U = y(s = N)$, ending up with

$$\beta = 1 - \gamma^N - (N-1)(1-\gamma)\gamma^{N-1} \quad . \tag{5}$$

Often, we are interested only in the upper tolerance limits, in this case, by choosing $L = y(r = 0) = -\infty$ and $U = y(s = N)$, the one-sided tolerance limit formula is obtained,

$$\beta = 1 - \gamma^N \quad . \tag{6}$$

In addition, the formulation was also extended to the more general case of $p$ output variables, i.e., $\vec{y} = (y_1, \ldots, y_p)$. In this case, for the one-sided tolerance limit, we have[18]

$$\beta = \sum_{j=0}^{N-p} \frac{N!}{(N-j)!j!}\gamma^j(1-\gamma)^{N-j} \quad . \tag{7}$$

### II.A.3. Probabilistic Propagation of Input Uncertainties Method for UQ Analyses

The application of the probabilistic propagation of input uncertainties method to perform a UQ analysis makes use of

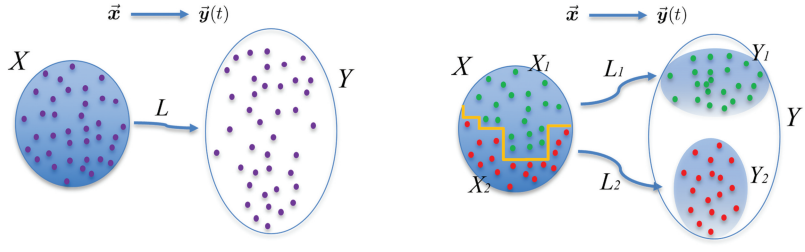


Fig. 1. Schematic representations of (left) nonchaotic and (right) chaotic behaviors of a system.

the Wilks confidence interval formula to determine the minimum sampling size $N$.[5,10,20] When applied to code simulations, as a first step, the input vector $\vec{x}$ is defined by selecting the relevant input uncertain parameters to the simulation. Each parameter is characterized by a reference value and a PDF. The output parameters of the study, usually called FOMs, should be selected as well.

On the base of the case study (e.g., single/multiple output, one-/two-sided tolerance limit), the proper Wilks formula is used to determine the minimum sampling size based on the chosen values of probability content and confidence level. Therefore, a Monte Carlo sampling of the input parameters is performed to obtain the sets of values that will be used as input to the $N$ code calculations. An advantage of the present method is that the sampling size is not influenced by the number of input uncertain parameters.

#### II.A.4. Correlation and Sensitivity Analysis

The results of the code runs can be subjected to a sensitivity analysis aimed at characterizing the importance of each input uncertain parameter on the uncertainty of each output FOM.[15,20] This analysis can be performed by calculating correlation or sensitivity coefficients. Commonly used are Pearson and Spearman correlation coefficients, which, respectively, characterize the linear and the monotonic correlation between an input parameter and a FOM. Linear regression coefficients are also commonly used in sensitivity analyses.

### II.B. Automatic LS Search

#### II.B.1. LS Definition

Considering again the deterministic nonlinear operator $L(t)$ representing the code simulation such that $\vec{y}(t) = L(t)\vec{x}$, the goal function $C$ can be introduced, which is a binary function that can assume either the value 0 (e.g., system failure) or 1 (e.g., system success) based on the response of the system $\vec{y}(t)$.[21] Hence, without the loss of generality, let us define $C$ such that it does not depend on time, i.e.,

$$C = C(\vec{y}) = \int_{t_0}^{t_{end}} C(\vec{y}(t))dt = \int_{t_0}^{t_{end}} C(L(t)\vec{x})\,dt = C(\vec{x}) \quad . \tag{8}$$

With this definition, it is possible to identify a subdomain of the input set $X$ leading to a specific output of the goal function. For example, the failure region $X_F$ can be defined as the subdomain of $X$ where $C = 0$. Hence, the success region $X_S$ will be complementary, i.e., $X_F$. $X_s = X$. In this case, we call LS the boundary surface in $X$ separating $X_F$ from $X_S$.

#### II.B.2. LS Application to System Bifurcations

At this point, a connection can be done to the definition of chaotic behavior of a system, as reported in Sec. II.A.1. In this view, we can consider a system (e.g., a SA code simulation) characterized by an output variable that splits into disjoint sets upon sampling from the input uncertainty set $X$ (see Fig. 1). In this case, according to Ref. [18], the statistic of the Wilks formula will not hold if applied on the whole $X$.

In this context, it might be possible to define a goal function $C$ in such a way that the subsets of $X$ that it identifies (e.g., $X_F$ and $X_C$) match those generated by the bifurcation in the system. In this way, the code operator $L(t)$ might be smooth in at least one of the subsets identified. Therefore, upon determination of the LS surface, it becomes possible to know the boundaries of the input domains on which the Wilks formula could be separately applied.

In general, and in addition to this possibility, in cases where a SA code application exhibits a phenomenological bifurcation/cliff-edge effect, the identification of the input parameter values that drive the transition between phenomena (i.e., the LS location) can always be of significant interest.

The methodology proposed in the present work for the identification of LS in the case of output bifurcation is presented in the following section.

#### II.B.3. Adaptative Sampling LS Search Method of RAVEN

The LS search algorithm of the Risk Analysis and Virtual Environment (RAVEN) (tool is introduced in Sec. II.C.2) is based on an adaptative-sampling strategy.[21–23] Ideally, the identification of the LS location with a pure Monte Carlo approach would need the evaluation of the system response in the full input domain of uncertainty $X$, i.e., performing an infinite number of calculations, which obviously is not feasible. A first, more reasonable approximation consists of locating the LS on a Cartesian N-D grid defined in $X$. In this way, the location of the LS will not be exactly known, but rather bounded as determined by those nodes between which the transition 0 to 1 of the goal function takes place, as in the left image in Fig. 2. Therefore, in this case, the LS identification would require computing a simulation on each node of the N-D grid that, for a good grid resolution, would still mean too high of a computational cost.

A more efficient process adopted in RAVEN uses a predicting model based on a supervised machine learning

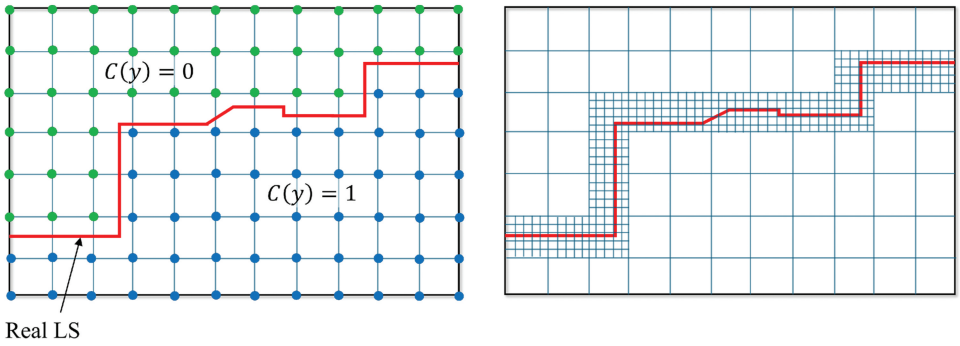


Fig. 2. Example of LS identification in a grid defined in a (left) 2D domain and (right) grid refinement.

(ML) algorithm of the classified type (taking only the integer output, e.g. 0 to 1). In the method, a reduced-order model (ROM) is trained to predict the outcome of the code simulation (in terms of the goal function $C(\vec{x})$) by using the values of the already performed calculations. In this way, the prediction of the LS location is used to choose the next nodes in the N-D grid that needs to be explored in order to efficiently improve the knowledge of the LS location (i.e. adaptative sampling).

This iterative process, using an active learning approach, can be repeated until the prediction of the ML model does not improve by further increasing the training set (performed calculation). More details about the iterative LS search algorithm is described by the scheme in Fig. 3.

Regarding the choice of the following nodes to be investigated, the metric used in RAVEN is based on the distance between the already performed evaluations and the LS predicted at the current iteration by the ROM.[21] In particular, the points are ranked on the basis of the following:

1. The distance to the predicted LS (the larger the distance is, the higher the score is for the candidate point).

2. The persistence (the larger is the number of times the prediction of the goal function for that point has changed, the higher is the score).

This approach establishes a queue of candidate points, with the quantity investigated given by the number of calculations performed in parallel.

With respect to the scheme in Fig. 3, the RAVEN algorithm requires that the convergence criterion be reached after a certain number (user selected) of consecutive iterations to end the iterative process. This is done to mitigate the effect of nonlinear bias occurring in the search, e.g., the algorithm might focus too much on a certain region while ignoring other zones, and hence, completely hide undiscovered parts of the LS.

In addition, the RAVEN algorithm for LS search improves the scheme presented by adding the possibility to accelerate the process by means of an adaptive refined multigrid approach. More details on the refined multigrid approach can be found in Refs. [21,23]. A representation of a refined grid is reported in the right image in Fig. 2.

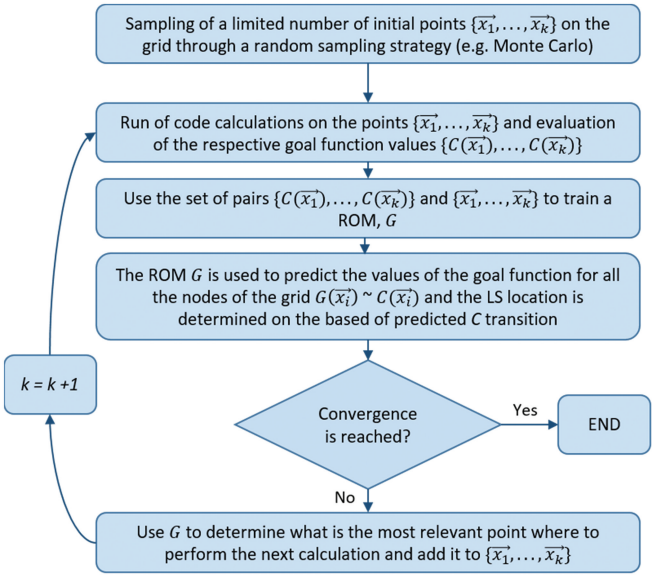


Fig. 3. Scheme of iterative LS search algorithm in RAVEN.

### II.B.4. Support Vector Machine ROM

As described previously, the LS search algorithm leverages an ML model to train a ROM that predicts the code response in the input domain. More specifically, it predicts the LS position by predicting the response of the binary goal function $C(\vec{x})$ at the points of the input domain.

The ML algorithm that was used in the present work is a support vector machine for binary classification, adopting a "rbf" (exponential) type kernel.[21] The support vector machine is a robust and fast running supervised ML model

aimed at determining the optimal separation hyperplane between data sets having different labels, and it features the best performance in binary classification problems. The support vector machine model implemented in RAVEN make use of the Scikit-learn library of Python.[24] A similar model application to the one of the current work is described in Ref. [23], and some different applications can be found in Ref. [25].

It should be said that many other supervised ML algorithms for binary classification can be used in support of the presented method to train the ROM (e.g., decision trees, neighbor class).

## II.C. Codes and Tools

### II.C.1. ASTEC Code

The ASTEC code, developed by the French Institut de Radioprotection et de Sûreté Nucléaire (IRSN),[2,26] is aimed at the comprehensive simulation of SA sequences in water-cooled NPPs, encompassing the SA from the initiating event to source term assessments.[a] The modular structure of ASTEC partitions the competency of each code module to simulate specific physical phenomena or reactor zones.

Specifically, with respect to the modules used in the present work, CESAR manages the thermal hydraulics of the coolant circuits, using a six-equation, two-phase thermal-hydraulic model. The ICARE module models the reactor core geometry and degradation phenomena. The two modules are tightly coupled in a SA sequence simulation. Applications of the ASTEC code extend across source term evaluation, probabilistic safety assessment, accident management studies, and more. ASTEC code version v2.2 beta was used in the present work (study carried out with ASTEC V2, IRSN all rights reserved [2022]).

### II.C.2. RAVEN Tool

The RAVEN[21] tool is a multipurpose software developed by Idaho National Laboratory starting from 2012. It is developed in Python as an open-source code using an object-oriented approach. It includes tools, algorithms, and models for probabilistic studies, and it is designed to perform classical and more advanced statistical analyses, parametric studies, LS determination, ML with artificial intelligence algorithms, etc. Parallel calculations, for both standard and high performance computing systems, are also fully managed.

[a] This study carried out with ASTEC V2, IRSN all rights reserved (2022).

### II.C.3. RAVEN-ASTEC Coupling

Since RAVEN does not have a dedicated coupling interface for ASTEC, the coupling was realized by developing a specific Python interface that was embedded in the RAVEN source code.[27] The new interface has the same features of the "generic" interface of RAVEN, with the addition that the software is able to locate the output file of ASTEC and inspect its content to understand if a simulation has successfully ended or it failed. This is a key advantage in the case of UQ studies, where failed calculation results must be identified and discarded from the statistics. The code coupling is completed by properly modifying the input file of ASTEC as required by RAVEN and setting up the input XML file to RAVEN.

In the case of a UQ analysis, RAVEN is able to drive the process needed for the study, retrieving instructions from the XML file. Accordingly, with the probabilistic propagation of input uncertainties method described in Sec. II.A.3, the coupling does the following:

1. Provides the sampling size N. RAVEN samples the values of the selected input uncertain parameters.

2. Creates a set of *N* different ASTEC input decks of the same sequence by using the sampled values.

3. Launches the code simulations on the base of the instructions provided.

4. Collects the simulations results and creates summary results files.

The ASTEC-RAVEN coupling workflow for UQ analysis is schematized in Fig. 4. More details are available in Ref. [27].

# III. CASE STUDY

## III.A. ASTEC Simulation of QUENCH-06 Experiment

### III.A.1. QUENCH-06 Experiment

The QUENCH test-6 experimental facility,[28] hosted in the Institute for Applied Materials Physics of KIT (Karlsruhe Institute of Technology), was designed to investigate the behavior of hot light water reactor fuel in quenching conditions. The test section consists of a rod bundle, including 21 fuel rod simulators surrounded by a shroud of Zircaloy, an insulation, and an external stainless steel cooling-jacket. A total of 20 rods are electrically heated, while the unheated rod is filled with $ZrO_2$ pellets and placed at the middle of the bundle. In addition, four Zr "corner rods,"

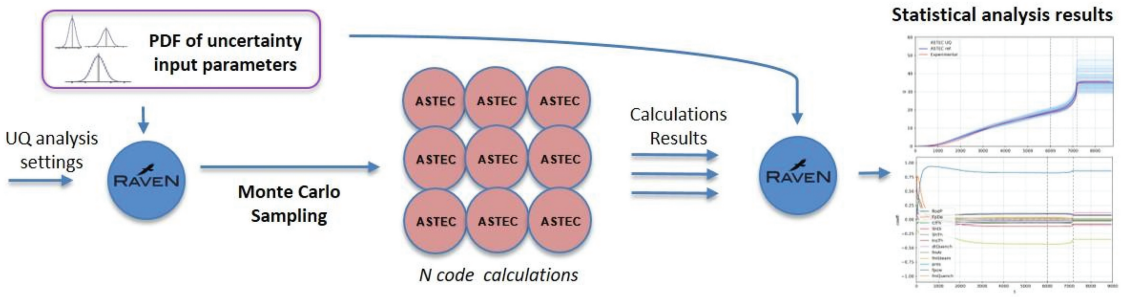


Fig. 4. Scheme of ASTEC-RAVEN coupling workflow for UQ analysis.[27]

located at the bundle corners, host most of the instrumentation. The test section is sealed by top and bottom plates, and the rods are supported by spacer grids.

Steam and argon enter from the bottom, move along the bundle, and then exit at the top end, where diagnostic instrumentation is located. The quenching water enters in the test section through a bottom line. A more detailed description of the QUENCH test-6 arrangement can be found in Ref. [28]. The experimental sequence lasts for about 9000 s and can be considered characterized by three phenomenological windows (PhWs):

1. *Pre-oxidation PhW*: This PhW is from the start of the sequence up to 6011 s, during which the electric power is increased until reaching a temperature plateau, partially pre-oxidizing the Zr.

2. *Heating-up PhW*: In this PhW, the electric power is increased with a ramp until the first injection of quenching water at 7179 s.

3. *Quenching PhW*: This PhW is from the start of water injection (7179 s) to the end of the experiment (after 9000 s).

The main events of the experiment are summarized in Table I, and a more exhaustive description can be found in Refs. [15,28].

### III.A.2. ASTEC Nodalization of QUENCH-06

The nodalization of the experimental setup was realized with the ICARE and CESAR modules, which are able to simulate thermal-hydraulic and early core degradation phenomena.[15] The domain is radially divided in two coaxial fluid channels, as shown in the right image in Fig. 5. The nine innermost rods are located inside the inner channel and collapse into a single representative rod. The remaining 12 rods are collapsed into another rod and located inside the outer channel, as are the four corner rods.

TABLE I

Summary of Main Events Characterizing the QUENCH Test-6 Sequence

| Time (s) | Events | PhW |
|---|---|---|
| 0 | Bundle at T = ~870 K; Ar and steam bottom injection (~3 g/s both) | Pre-oxidation |
| 30 | Start of heating up to ~1473 K | |
| 1965 | Start of steady temperature oxidation at ~1473 K | |
| 6011 | Start of heat-up phase | Heating up |
| 6620 | Extraction of corner rod B from the bundle | |
| ~7200 | Onset of temperature escalations and of significant $H_2$ production | |
| 7179 | Shutoff of steam and Ar bottom injection; start of quenching with the water "pre-injection" (4 L in 5 s); rod failure in the experiment | Quenching |
| 7180 | Shroud failure in the experiment | |
| 7205 | Start of electric power reduction from 18.2 to 3.9 kW | |
| 7215 | Start of water main injection (time-dependent mass flow rate) | |
| 7221 | Electric power at 3.9 kW | |
| ~7431 | Electric power shutoff; main water shutoff | |
| 9000 | End of the test | |

The model also includes grid spacers, plates, shroud, insulation, and the external cooling jacket. It is axially divided into equal slices of 55 mm in height. The ASTEC model is described with more details in Refs. [9,15].

### III.A.3. Best-Estimate Simulation of QUENCH-06 Sequence

The simulation of the experimental sequence was carried out with ASTEC code v2.2b, with a calculation timing of about 10 min. The detailed output results are compared against the experimental data in Refs. [9,15]. From the time-dependent quantitative accuracy evaluation, carried out in Ref. [15], it was concluded that the code featured a very good prediction in the pre-oxidation and the heating-up PhWs. In the quenching PhW, some discrepancies were observed, but the general accuracy was evaluated as good. The $H_2$ mass produced along the sequence and the shroud temperature are reported in Fig. 6. Figure 7 reports the axial profiles of the $ZrO_2$ thickness in the corner rods and in the heated rods at the end of the test.

A key point for the present work is the ASTEC prediction of the bundle structural status. The simulation captured a local melting of materials at the most heated-up level without the loss of component integrity (see Fig. 8), similar to what was observed in the post-experiment analysis: local melting occurred, without a major loss of structures integrity.[28] The presence of solid layers of $ZrO_2$ and ZrO ensured that the condition of loss of integrity was not reached, preventing any material relocation.[15]

## III.B. UQ Analysis of the ASTEC Simulation

A UQ analysis of the code simulation was carried out through the RAVEN-ASTEC coupling and by applying the probabilistic propagation of input uncertainties method described in Sec. II.A.3. While the study was reported in detail in Ref. [15], the key elements and outcomes to be used as starting points for the present application are summarized in the following section.

### III.B.1. Setup of the UQ Analysis

A total of 23 uncertain input parameters to the code simulation were selected, including geometric data, initial and boundary conditions, integrity criteria, and heat transfer model parameters. The comprehensive list with the associated reference value and PDF can be found in Refs. [9,15]. The output FOMs selected were five parameters.

Following the methodology described in Sec. II.A.3, the number of code runs was defined based on the Wilks confidence interval formula. Hence, by considering the one-sided tolerance limit for five FOMs and imposing probability content and a confidence level of 95%, a minimum number of 181 calculations was obtained.[9,15] Accounting for possible code failures, the total number of simulations was raised to 200.

### III.B.2. Outcomes of the UQ Analysis

The uncertainty of the simulation was characterized in terms of width of the dispersion band of each FOM. In

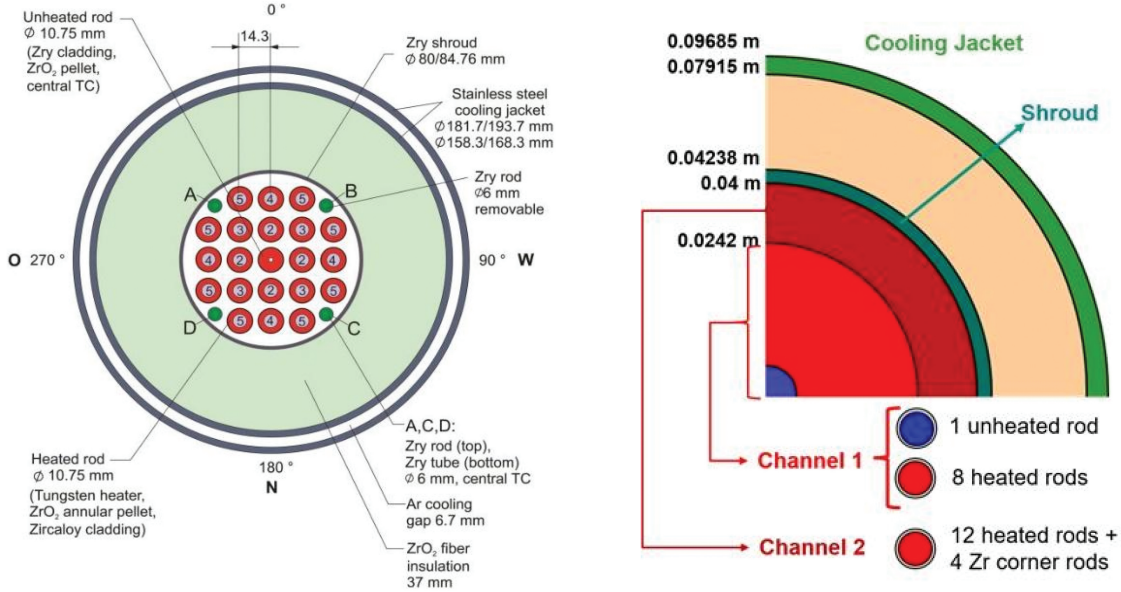


Fig. 5. Section of the (left) QUENCH-06 test section and (right) radial nodalization in ASTEC.[29]

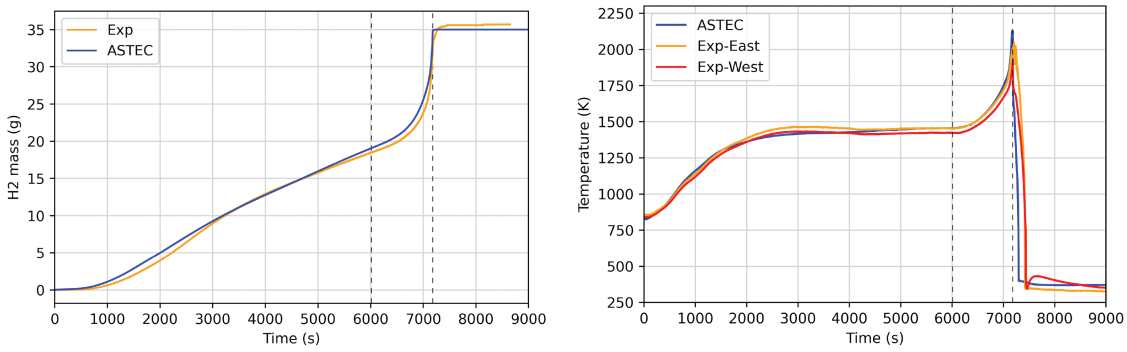


Fig. 6. (left) Mass produced $H_2$ and (right) shroud temperature at 950 mm of elevation from experimental and code data.

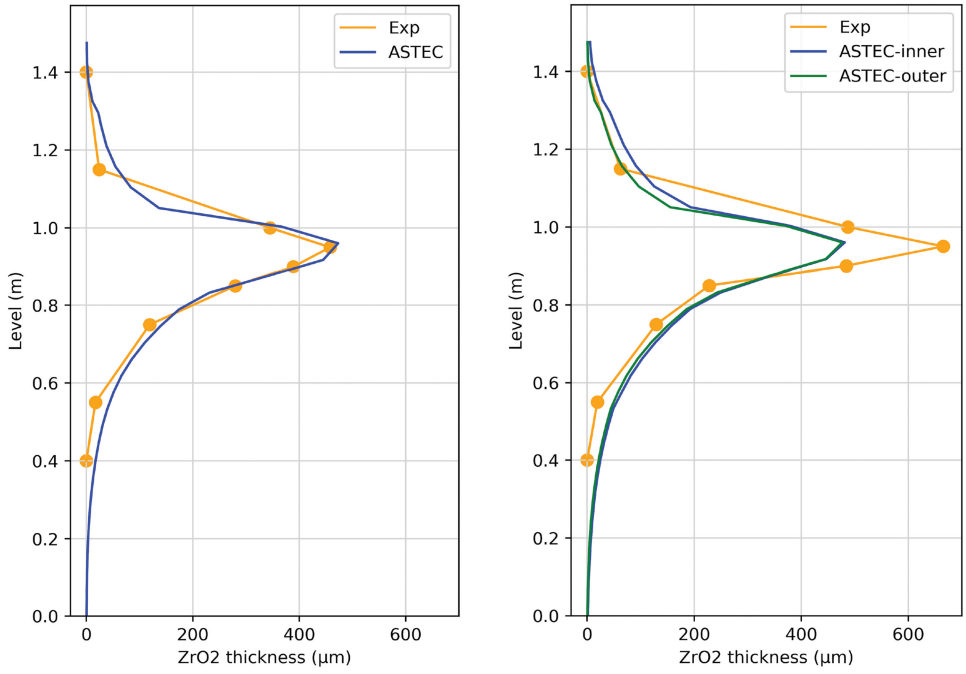


Fig. 7. Axial profile of $ZrO_2$ thickness averaged in the (left) corner rod cladding and (right) in the heated rod cladding at calculation end (9000 s) from experimental and code data.

general, a minor uncertainty was observed during the pre-oxidation phase, while uncertainty was observed to increase during bundle heating up and quenching. As an example, Fig. 9 reports the dispersion band of the $H_2$ mass produced. In Refs. [9,15], this behavior was partially attributed to the nonlinear evolution of the Zr oxidation reaction at temperatures above 1770 K.

A key outcome of this study was that a reason for the general output uncertainty spread could be attributed to a phenomenology bifurcation that took place. Indeed, since the conditions for loss of integrity of the cladding were very close to be reached in the reference simulation (see Fig. 8), the perturbation introduced by the uncertain parameters sampling made that a part of the UQ simulations ended up to localized cladding failure and material relocation.

This point is evinced in Fig. 10, which shows the rod material composition and status after quenching for two simulations of the 200 picked up at the two extremes: the lowest and the highest heating cases. The scenario in the left image in Fig. 10 features no melting of materials, while the one on the right is characterized by localized melting and relocation around the 9.50-m elevation.

A consequence of this phenomenological bifurcation was the separation of one of the selected output FOMs into disjoint sets. This can be observed in the right image in Fig. 11, which shows the dispersion of the $ZrO_2$ profile in the internal ring heated-rod cladding at calculation end.

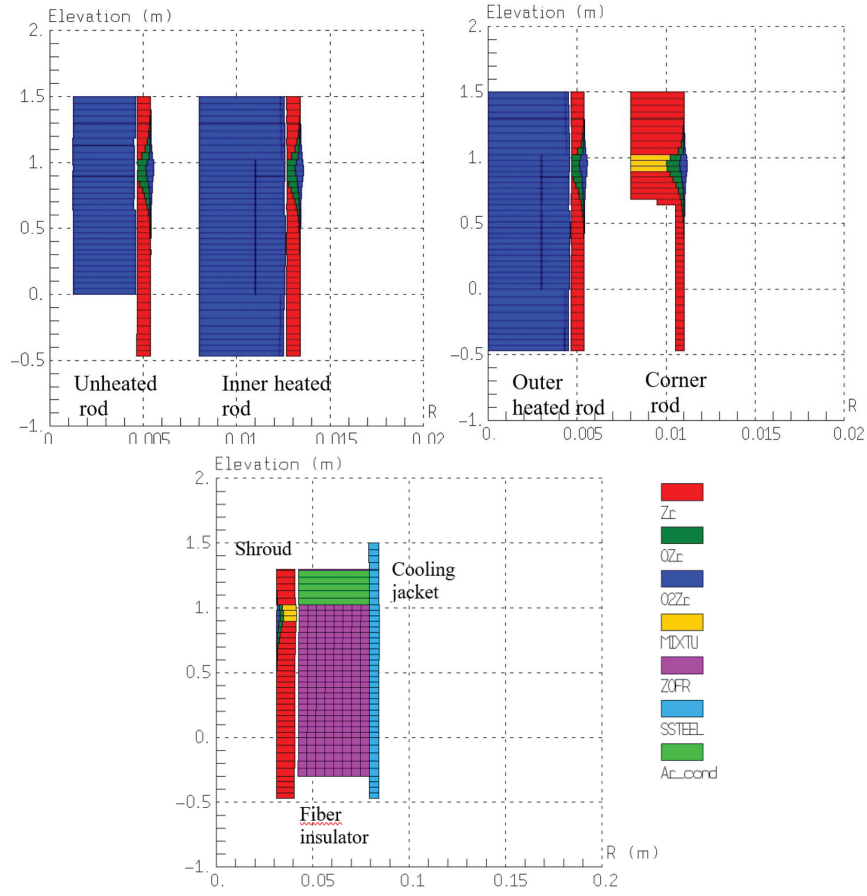


Fig. 8. (top left) Nodalization of inner ring rods, (top right) outer ring rods, and (bottom) shroud with materials at calculation end (9000 s) of ASTEC simulation.

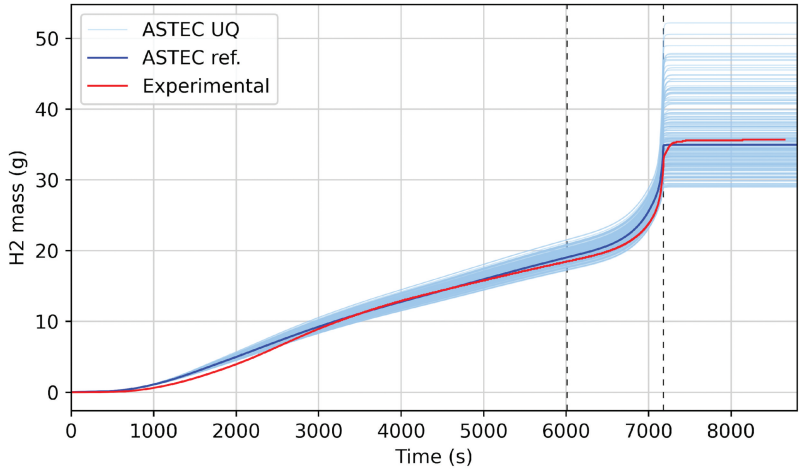


Fig. 9. Dispersion band of $H_2$ cumulative mass against experimental and best-estimate results.

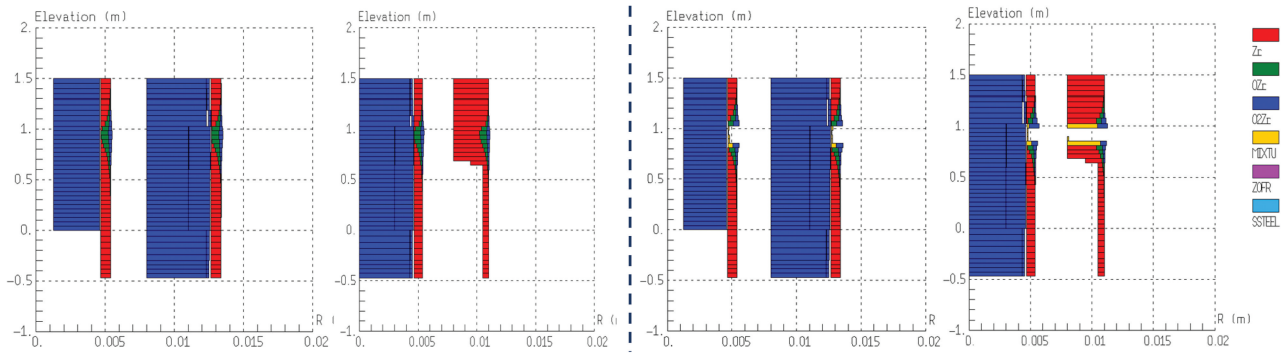


Fig. 10. Material and status of rod components in the ASTEC simulation for (left) lowest oxidation result and (right) highest oxidation result after quenching occurrence.

In the right image in Fig. 11, it can be observed that, at the most oxidized elevations (0.80 to 1.15 m), a high spread of results affected the dispersion band of the $ZrO_2$ thickness. Furthermore, some results take on a value of 0 due to local cladding failure and material relocation, resulting in a complete separation from the dispersion band. This situation should be considered as a bifurcation of the output domain of this FOM due to the cliff-edge effect of the bundle degradation phenomenology.

### III.C. Application of Adaptative Sampling LS Search

In Sec. II.A.2, it was underlined that the assumptions of the Wilks formula should be considered not respected for those FOMs ending up in bifurcations (i.e., chaotic behavior). In this case, as proposed in Sec. II.B.2, the LS surface is determined within the input domain to distinguish the input parameter values that lead to different phenomena. This approach makes it possible to consider the Wilks formula as respected on each continuous side of the LS.

Considering the FOM bifurcation obtained in the UQ analysis of Sec. III.B, a proposed solution is to discern the input values that lead to a cladding loss of integrity to those that feature always intact structures. In other words, we may want to find the input conditions for which the simulation evolves to one of the two phenomenologies identified, which turns out to be a LS search problem.

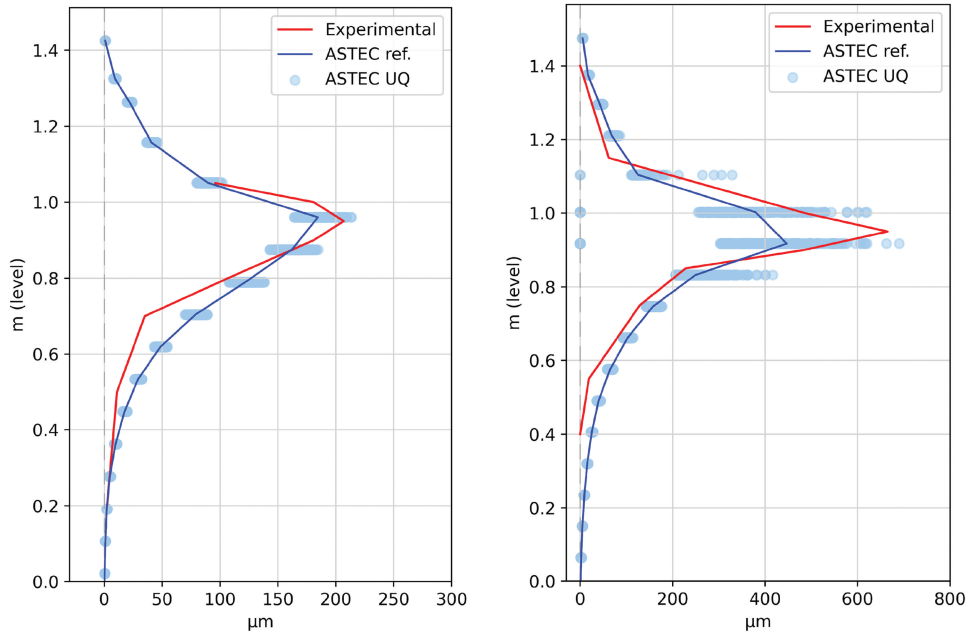


Fig. 11. Dispersion band of $ZrO_2$ profile in the (left) corner rod at 6620 s and (right) in the internal ring heated rod at calculation end against experimental and best-estimate results.

### III.C.1. Setup of LS Search Method

According to Sec. II.B, for the present application, it is possible to consider as binary goal function $C$ the final state of cladding, i.e., we set $C = 1$ for intact cladding, and $C = 0$ for failed cladding at calculation end. As mentioned, the LS method can be applied to multidimensional problems; yet, in order to reduce the computational effort, the number of input parameters was limited to the most relevant to our goal function. With this purpose, Spearman correlation coefficients were calculated between the 23 input uncertain parameters and the goal function for the 200 performed calculations. The results are reported in Fig. 12.

The coefficients captured a significant negative correlation with the electric power factor *fpow*, a moderate positive correlation with the steam mass flow rate *fmSteam*, and a moderate-low negative correlation with the timing of quenching *dtQuench*. The correlation with the other parameters was low or negligible. As a result of this, only the two most relevant input uncertain parameters were chosen to be used in the LS search problem, i.e., electric power and steam mass flow rate.

The LS search in RAVEN was applied by employing a support vector machine algorithm with a rbf-type kernel for the ROM training. Given the computational resources available, the number of parallel calculations was chosen to be 10 and the number of consecutive converging loops to determine the end of the research was selected to be eight. The adaptive multigrid approach was activated to guarantee the acceleration toward convergence and a higher LS resolution.

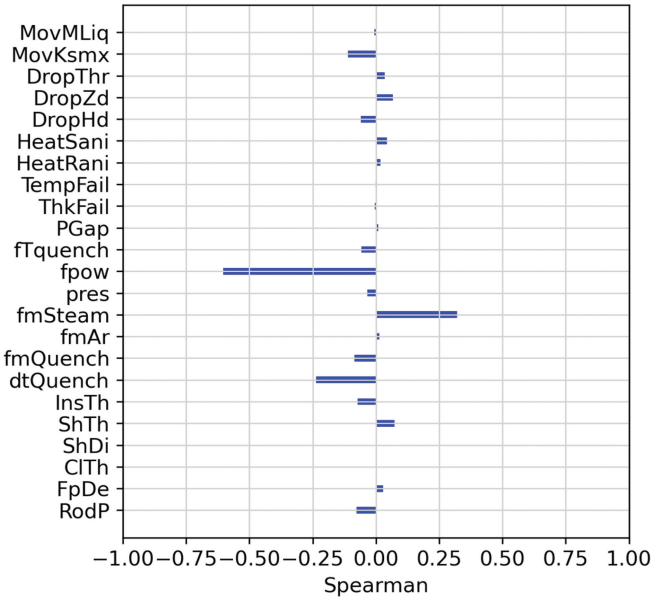


Fig. 12. Spearman coefficients between the goal function $C$ and the 23 input uncertain parameters.

In the example provided, disregarding the less relevant input parameters clearly constitutes an approximation. However, since these parameters are weakly correlated with the goal function, the approximation can be considered acceptable. In other applications, the number of input parameters must be carefully evaluated, taking into account the following factors:

1. Computational time required for each simulation
2. Available computational resources
3. Correlation between the parameters to be discarded and the goal function.

### III.C.2. Results of the LS Search

The LS search ended (achieving eight consecutive converging loops) at a total number of 180 ASTEC calculations without reporting any code failure. In Fig. 13, the algorithm's search results are shown in terms of the goal function $C$ calculated at the investigated points. Each calculation performed is reported in the two-dimensional (2D) input domain, and the corresponding value of the output goal function is expressed with colors: purple (dark) for failed cladding and yellow (light) for intact cladding. The input parameters on the two axes were normalized on their reference value.

It can be observed that the plot delimitates a boundary (LS) dividing the input domain in two zones for the two possible values of the goal function. The LS can be approximated as a straight line, crossing the $x$-axis at about 1.01 and the $y$-axis at about 1.003. The calculations located above the LS will result in the failure of cladding, while those having input values located below the LS will have final intact structures. Therefore, for results where the steam mass flow rate value (normalized) is higher than about 1.01, the cladding will always be intact, no matter the value assumed by the fuel electric power (within its adopted uncertainty range).

For points too close to the LS, the goal function result will not be known with good confidence. The higher the resolution of the LS needed and the higher the grid refinement, the higher the final number of calculations will be. The implemented algorithm allows for having a very good estimation of the LS position by using a limited number of calculations.

In the plot in Fig. 14, the color of the points is in this case refer to the order of execution of the calculation along the LS search. It can be observed that the first calculations (darker color) are randomly distributed in the input domain, while as the research advances, the following calculations converge on the LS line.

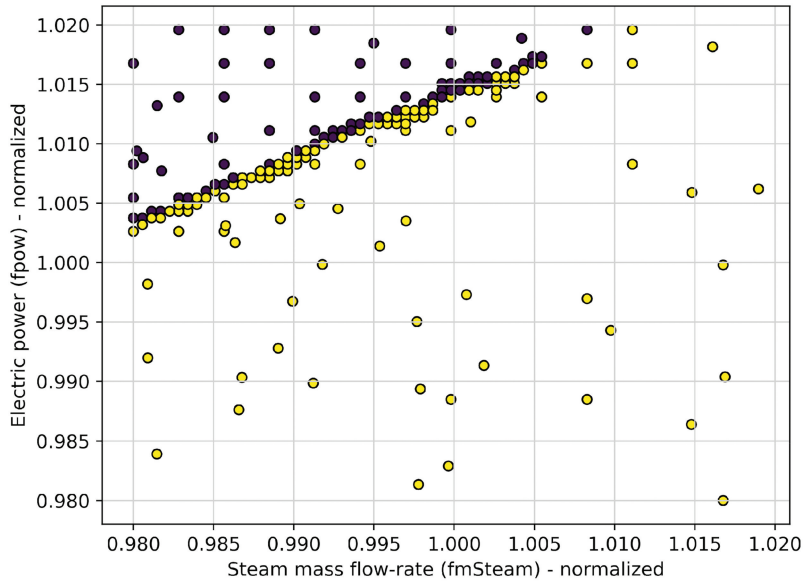


Fig. 13. Calculations executed in the LS search in terms of input values (normalized) and corresponding goal function value: purple (dark) for failed and yellow (light) for intact cladding.

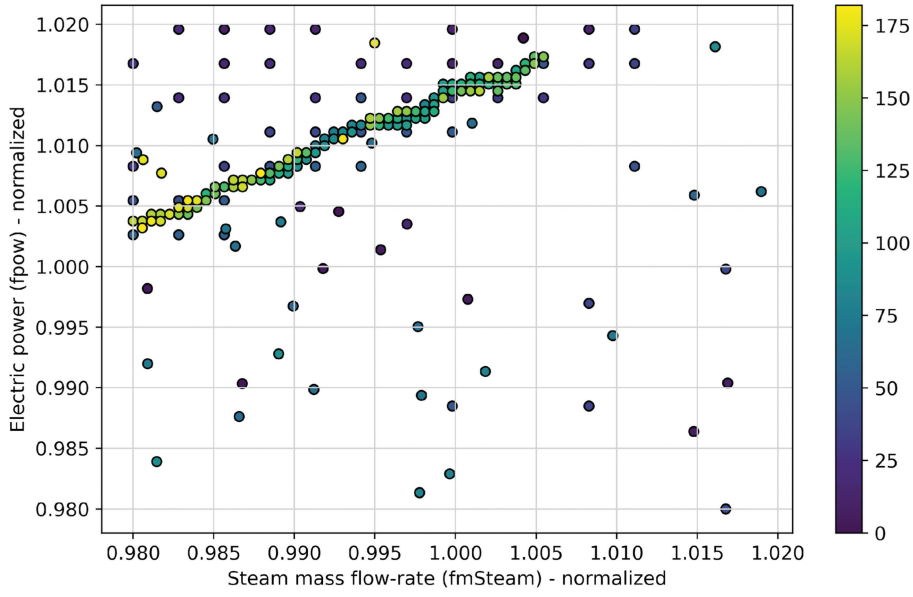


Fig. 14. Calculations executed in the LS search in terms of input values (normalized) and corresponding order of execution in a color scale.

## IV. CONCLUSIONS

The first aim of the present work was to highlight how the peculiarity of SA simulations may present a challenge for UQ application due to the presence of strongly nonlinear and discontinuous phenomena. Indeed, application of the probabilistic propagation of input uncertainties method to SA simulations often results in a spread of the output uncertainty, discontinuous behaviors, and even bifurcations of the FOMs into subsets. It is also stressed out, as in these cases, the statistics of the Wilks formula might not be respected on the whole domain of uncertainty,[18] thus making the method unusable.

In this scenario, in the present work, it was proposed that the application of the LS search method in RAVEN would be a useful strategy in support of UQ analyses evolving into a phenomenological bifurcation, i.e., separation of a FOM into disjoint subsets. This adaptative sampling method was used to identify the boundary between input the subdomains evolving to different phenomena. In this way, the Wilks formula might be considered to be respected on each identified input subdomain, provided it is smooth in this case.

The proposed case study dealt with the ASTEC code simulation of an experimental sequence involving early core degradation phenomena. Since in the reference simulation the bundle components were close to achieving loss-of-integrity conditions, the uncertainty introduced into the UQ analysis by input random sampling caused a localized cladding failure in part of the UQ simulations. This determined the separation of a FOM (i.e., $ZrO_2$ thickness in cladding).

The LS method was initiated by defining the goal function $C$ on the basis of the final state of cladding (intact vs. failed). The two most closely correlated input parameters were selected by calculating the Spearman correlation coefficients with the values of $C$. Therefore, the iterative LS method was applied by means of RAVEN-ASTEC coupling, selecting a support vector machine algorithm. A good convergence of the method was achieved in 180 simulations. The LS surface was outlined with a good resolution on the 2D input domain, identifying those input parameter values that led the simulation to evolve into one of the two phenomenologies identified.

The case study presented was an example with the ambition to propose a preliminary solution to a UQ study in which the statistics cannot be respected, as often happens in SA applications. In this context, the accurate identification of the input subsets evolving into different phenomena would already be considered a valuable result for many applications, as it adds relevant information to a chaotic system. Furthermore, in scenarios where it is necessary, such as UQ studies focused on statistically determining the safety limits of the system, a possible next step could involve applying the UQ specifically to one continuous side of the identified LS line. This approach should yield a more statistically robust solution.

While the method described requires a relevant number of additional numerical calculations, this computational effort can be justified by the precision and valuable insights it provides. Yet, it remains essential to assess the trade-off between computational cost and the added value on a case-by-case basis.

## Acronyms

2D: two dimensional

ASTEC: Accident Source Term Evaluation Code

CRP: coordinated research project

FOM: figure of merit

LS: limit surface

ML: machine learning

IRSN: Institut de Radioprotection et de Sûreté Nucléaire

NPP: nuclear power plant

PDF: probability distribution function

PhW: phenomenological window

ROM: reduced-order model

RAVEN: Risk Analysis and Virtual Environment

SA: severe accident

UQ: uncertainty quantification

## Disclosure Statement

No potential conflict of interest was reported by the author(s).


## Funding

This research was supported by the International Atomic Energy Agency under the CRP award I31033 on Advancing the State-of-Practice in Uncertainty and Sensitivity Methodologies for Severe Accident Analysis in Water Cooled Reactors, launched in 2019.



## ORCID

Pietro Maccari http://orcid.org/0000-0003-1521-9198


## References


1. J. P. VAN DORSSELAERE et al., "Integral Codes for Severe Accident Analyses," *Nuclear Safety in Light Water Reactors*, Ch. 8, p. 625, Academic Press, Waltham, Massachusetts (2012); https://doi.org/10.1016/B978-0-12-388446-6.00008-3.
2. P. CHATELARD et al., "Main Modelling Features of the ASTEC V2.1 Major Version," *Ann. Nucl. Energy*, **93**, 83 (2016); https://doi.org/10.1016/j.anucene.2015.12.026.
3. FAUSKE & ASSOCIATES, LLC, "Transmittal Document for MAAP5 Code Revision MAAP5.02," FAI/13-0801 (2013).
4. L. L. HUMPHRIES et al., "MELCOR Computer Code Manuals," SAND-2015-6692R, Sandia National Laboratories (2015); https://doi.org/10.2172/1433918.
5. F. S. D'AURIA et al., *Best Estimate Safety Analysis for Nuclear Power Plants: Uncertainty Evaluation*, Vol. 52, IAEA Safety Report Series, International Atomic Energy Agency, Vienna, Austria (2008); https://www.iaea.org/pub

lications/7768/best-estimate-safety-analysis-for-nuclear-power-plants-uncertainty-evaluation.

6. R. P. MARTIN et al., "Progress in International Best Estimate Plus Uncertainty Analysis Methodologies," *Nucl. Eng. Des.*, **374**, (Apr. 2021); https://doi.org/10.1016/j.nucengdes.2020.111033.

7. L. E. HERRANZ et al., "The EC MUSA Project on Management and Uncertainty of Severe Accidents: Main Pillars and Status," *Energies*, **14**, *15*, 4473 (2021); https://doi.org/10.3390/en14154473.

8. F. MASCARI et al. "Overview of IAEA CRP I31033: Advancing the State-of-Practice in Uncertainty and Sensitivity Methodologies for Severe Accident Analysis in Water Cooled Reactors," presented at the 10th European Review Mtg. on Severe Accident Research (ERMSAR2022), Akademiehotel, Karlsruhe, Germany, May 16–19, 2022.

9. "Advancing the State of the Practice in Uncertainty and Sensitivity Methodologies for Severe Accident Analysis in Water Cooled Reactors in the QUENCH-06 Experiment," IAEA-TECDOC-2045, 978-92-0-108524-5, International Atomic Energy Agency (2024); https://www-pub.iaea.org/MTCD/Publications/PDF/TE-2045web.pdf (accessed Nov. 2, 2024).

10. H. GLAESER, "GRS Method for Uncertainty and Sensitivity Evaluation of Code Results and Applications," *Sci. Technol. Nucl. Ins.*, **2008**, 1 (2008); https://doi.org/10.1155/2008/798901.

11. O. COINDREAU et al., "Uncertainty Quantification for a Severe Accident Sequence in a SFP in the Frame of the H-2020 Project MUSA: First Outcomes," *Ann. Nucl. Energy*, **188**, 109796 (2023); https://doi.org/10.1016/j.anucene.2023.109796.

12. F. MASCARI et al., "Main Outcomes of the Phebus FPT1 Uncertainty and Sensitivity Analysis in the EU-MUSA Project," *Ann. Nucl. Energy*, **196**, 110205 (2024); https://doi.org/10.1016/j.anucene.2023.110205.

13. R. P. MARTIN and A. PETRUZZI, "Progress in International Best Estimate Plus Uncertainty Analysis Methodologies," *Nucl. Eng. Des.*, **374**, 111033 (2021); https://doi.org/10.1016/j.nucengdes.2020.111033.

14. R. O. GAUNTT and P. D. MATTIE, "Fukushima Daiichi Unit 1 Accident Progression Uncertainty Analysis and Implications for Decommissioning of Fukushima Reactors—Volume I," SAND2016-0232, Sandia National Laboratories (2016).

15. P. MACCARI et al., "Validation and Uncertainty Analysis of ASTEC in Early Degradation Phase Against QUENCH-06 Experiment," *Nucl. Eng. Des.*, **414**, 112600 (2023); https://doi.org/10.1016/j.nucengdes.2023.112600.

16. S. S. WILKS, "Determination of Sample Sizes for Setting Tolerance Limits," *Ann. Math. Statist.*, **12**, *1*, 91 (1941); https://doi.org/10.1214/aoms/1177731788.

17. S. S. WILKS, "Statistical Prediction with Special Reference to the Problem of Tolerance Limits," *Ann. Math. Statist.*, **13**, *4*, 400 (1942); https://doi.org/10.1214/aoms/1177731537.

18. A. GUBA, M. MAKAI, and L. PÀL, "Statistical Aspects of Best Estimate method—I," *Reliab. Eng. Syst. Saf.*, **80**, *3*, 217 (2003); https://doi.org/10.1016/S0951-8320(03)00022-X.

19. D. H. SATTINGER, *Group Theoretic Methods in Bifurcation Theory*, Vol. 762, Springer Minneapolis, Minnesota (2006); https://books.google.com/books?hl=it&lr=&id=hqN6CwAAQBAJ&oi=fnd&pg=PA1&dq=D.+H.+Sattinger,+Group+theoretic+methods+in+bifurcation+theory.+Springer,+vol.+762,+2006&ots=qSgGoF-zHS&sig=97pSoe5OiqegK8naWuXOxNNVYlA.

20. A. BERSANO et al., "Ingress of Coolant Event Simulation with Trace Code with Accuracy Evaluation and Coupled DAKOTA Uncertainty Analysis," *Fusion Eng. Des.*, **159**, 111944 (2020); https://doi.org/10.1016/j.fusengdes.2020.111944.

21. A. ALFONSI et al., "RAVEN Theory Manual," INL/EXT-16-38178, Idaho National Laboratory (Apr. 2020).

22. M. D'ONORIO et al., "Nuclear Safety Enhanced: A Deep Dive into Current and Future RAVEN Applications," *Nucl. Eng. Des.*, **427**, 113422 (2024); https://doi.org/10.1016/j.nucengdes.2024.113422.

23. C. PARISI et al., "Automatic Limit Surface Search for PWR Transients by RELAP5-3D/RAVEN Codes," INL/CON-18-45361-Rev000, Idaho National Laboratory (2018).

24. "Machine Learning in Python," scikit-learn; https://scikit-learn.org/stable/ (accessed Nov. 2, 2024).

25. J. WANG, Q. CHEN, and Y. CHEN, "RBF Kernel Based Support Vector Machine with Universal Approximation and Its Application," *Proc. International Symp. on Neural Networks*, pp. 512–517, Springer (2024).

26. P. CHATELARD et al., "ASTEC V2 Severe Accident Integral Code Main Features, Current V2.0 Modelling Status, Perspectives," *Nucl. Eng. Des.*, **272**, 119 (2014); https://doi.org/10.1016/j.nucengdes.2013.06.040.

27. P. MACCARI et al., "ASTEC-RAVEN Coupling for Uncertainty Analysis of an Ingress of Coolant Event in Fusion Plants," *Fusion Eng. Des.*, **169**, 112442 (2021); https://doi.org/10.1016/j.fusengdes.2021.112442.

28. L. SEPOLD et al., "*Experimental and Computational Results of the QUENCH-06 Test (OECD ISP-45)*," FZKA-6664, Forschungszentrum Karlsruhe GmbH Technik und Umwelt (Germany) (2004).

29. F. GABRIELLI et al., "Validation of the ASTEC Integral Code Using the QUENCH-06 and QUENCH-08 Experiments," *Proc. 9th European Review Mtg. on Severe Accident Research* (*ERMSAR2019*), Prague, Czech Republic, March 18–20, 2019.